

1997

An experimental study of the response of a microphone mounted in a flat plate

Hedayat U. Hamid
San Jose State University

Follow this and additional works at: https://scholarworks.sjsu.edu/etd_theses

Recommended Citation

Hamid, Hedayat U., "An experimental study of the response of a microphone mounted in a flat plate" (1997). *Master's Theses*. 1447.
DOI: <https://doi.org/10.31979/etd.y9wn-kpw7>
https://scholarworks.sjsu.edu/etd_theses/1447

This Thesis is brought to you for free and open access by the Master's Theses and Graduate Research at SJSU ScholarWorks. It has been accepted for inclusion in Master's Theses by an authorized administrator of SJSU ScholarWorks. For more information, please contact scholarworks@sjsu.edu.

INFORMATION TO USERS

This manuscript has been reproduced from the microfilm master. UMI films the text directly from the original or copy submitted. Thus, some thesis and dissertation copies are in typewriter face, while others may be from any type of computer printer.

The quality of this reproduction is dependent upon the quality of the copy submitted. Broken or indistinct print, colored or poor quality illustrations and photographs, print bleedthrough, substandard margins, and improper alignment can adversely affect reproduction.

In the unlikely event that the author did not send UMI a complete manuscript and there are missing pages, these will be noted. Also, if unauthorized copyright material had to be removed, a note will indicate the deletion.

Oversize materials (e.g., maps, drawings, charts) are reproduced by sectioning the original, beginning at the upper left-hand corner and continuing from left to right in equal sections with small overlaps. Each original is also photographed in one exposure and is included in reduced form at the back of the book.

Photographs included in the original manuscript have been reproduced xerographically in this copy. Higher quality 6" x 9" black and white photographic prints are available for any photographs or illustrations appearing in this copy for an additional charge. Contact UMI directly to order.

UMI

A Bell & Howell Information Company
300 North Zeeb Road, Ann Arbor MI 48106-1346 USA
313/761-4700 800/521-0600

**AN EXPERIMENTAL STUDY OF THE RESPONSE OF A
MICROPHONE MOUNTED IN A FLAT PLATE**

A Thesis

Presented to

**The Faculty of the Department of
Mechanical and Aerospace Engineering
San Jose State University**

In Partial Fulfillment

of the Requirements for the Degree

Master of Science

by

Hedayat U. Hamid

May 1997


UMI Number: 1384696

UMI Microform 1384696
Copyright 1997, by UMI Company. All rights reserved.

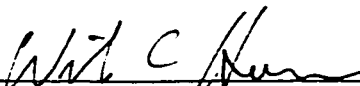
**This microform edition is protected against unauthorized
copying under Title 17, United States Code.**

UMI
300 North Zeeb Road
Ann Arbor, MI 48103


APPROVED FOR THE DEPARTMENT OF MECHANICAL
AND AEROSPACE ENGINEERING

 4-9-1997

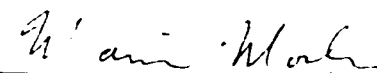
Dr. Nikos J. Mourtos
Department of Mechanical & Aerospace Engineering

 4-9-97

Dr. William C. Horne
NASA Ames Research Center

 Seto APRIL 9, 1997

Professor William Seto
Department of Mechanical & Aerospace Engineering

 4 9 97

Dr. Marianne Mosher
NASA Ames Research Center

APPROVED FOR THE UNIVERSITY



© 1997

Hedayat U. Hamid

ALL RIGHTS RESERVED

ABSTRACT

AN EXPERIMENTAL STUDY OF THE RESPONSE OF A MICROPHONE MOUNTED IN A FLAT PLATE

by Hedayat U. Hamid

An experimental investigation of the acoustic response of a single microphone mounted in a flat plate was conducted without flow in the anechoic chamber at NASA Ames Research Center. The purpose was to obtain detailed understanding of the acoustic response due to the various microphone installations, including flush-mount and recess-mount configurations.

The deep recess mount configuration showed results with unacceptably large oscillations. Large oscillations and detrimental resonances were also seen in installation configurations which either used the porous screen or the protection grid. The results from the 1 mm and the 0.5 mm recess, bare microphone diaphragm configurations suggest that flush-mount, bare microphone configurations have the most regular magnitude and phase response to an external source. The response of the baseline configuration relative to a free field microphone was also conducted and a sound pressure level increase of 6 dB, as predicted by theory, was obtained.

ACKNOWLEDGMENTS

This work has been supported by NASA Ames Research Center. The author would like to thank Dr. Clif Home, Dr. Marianne Mosher, Mr. Paul Soderman, and other members of the Low Speed Aerodynamics Branch for their guidance and support while this research was being conducted. I would also like to thank Dr. Nikos Mourtos and Professor William Seto of San Jose State University for their advice and encouragement throughout my experience as a student. Finally, and most importantly, I would like to thank my parents and the rest of my family for providing support and confidence.

TABLE OF CONTENTS

Title page	i
Copyright page	ii
Signature page	iii
ABSTRACT	iv
ACKNOWLEDGMENTS	v
TABLE OF CONTENTS	vi
NOMENCLATURE	viii
TABLE OF FIGURES	xi
1. INTRODUCTION	1
2. EXPERIMENTAL APPROACH	7
2.1 Test Setup and Instrumentation	7
2.2 Apparatus Construction and Mounting	10
2.3 Analysis Method	11
2.4 Measurement Accuracy and Experimental Error	14
3. RESULTS AND DISCUSSION	24
3.1 Effects of Deep Recess Configuration	24
3.2 Effects of Flush-Mount Configurations	25
3.2.1 <i>Flush-Mounted Grid</i>	25
3.2.2 <i>Flush-Mounted Grid Behind Porous Screen</i>	26
3.2.3 <i>Protrusion of Mic Grid to Allow Flush Diaphragm</i>	27

3.3 Effects of Shallow-Mount Configurations	28
3.3.1 1 mm Recess Mic with Grid	28
3.3.2 1 mm Recess Mic with Grid Behind Porous Screen	29
3.3.3 1 mm Recess Bare Mic Diaphragm	30
4. PLANE-WAVE REFLECTION AT PANEL SURFACE	37
4.1 Overview	37
4.2 Theory: Plane-Wave Reflections	38
4.3 Results and Discussion	40
5. SOUND TUBE MEASUREMENTS	43
5.1 Sound Tube Test Setup	43
5.2 Theoretical Basis for Measurement	44
5.3 Results and Discussion	45
5.3.1 Empty Tube	45
5.3.2 Fiberglass Sample	46
5.3.3 Three-half-inch Thick Foam	46
5.3.4 Acoustically Transparent (Porous) Screen	46
5.3.5 Foam and Porous Screen Combination	47
6. CONCLUSIONS	50
REFERENCES	52

NOMENCLATURE

English Letter Symbols:

A	amplitude, incident sound pressure, Pa
B	amplitude, reflected sound pressure, Pa
c	speed of sound, m/s
f	frequency, Hz
$G_{xx}(f)$	power spectrum of the reference microphone
$G_{xy}(f)$	cross-spectrum between reference and test microphone
$H(f)$	transfer function
$H(f)_{\substack{\text{baseline} \\ \text{ref}}}$	transfer function of baseline configuration relative to the fixed mic
$H(f)_{\substack{\text{installation} \\ \text{ref}}}$	transfer function of installation configuration relative to the fixed mic
$H(f)_{\substack{\text{installation} \\ \text{baseline}}}$	transfer function of installation configuration relative to baseline configuration
L_p	sound pressure level, dB
L_{p_i}	incident sound pressure level, dB
L_{p_s}	sound pressure level at a surface, dB
P	sound pressure, Pa
P_i	incident sound pressure, Pa
P_r	reflected sound pressure, Pa

P_{ref}	reference pressure (= 20 μ Pa), Pa
P_s	sound pressure at a surface, Pa
t	time, s
T	air temperature, $^{\circ}$ C

Greek Letter Symbols:

α	sound absorption coefficient
$\gamma_{xy}^2(f)$	coherence function between the reference and the test microphones
λ	wavelength, m
n_d	number of averages
μ	micro (10^{-6})
θ_I	incident wave angle, degrees
θ_R	reflected wave angle, degrees
ω	phase angle, degree

Unit/Dimension Symbols:

C	Celsius
dB	decibel
ft	foot

Hz	Hertz, cycles/s
F	Fahrenheit
in	inch
K	Kelvin
m	meter
Rayl	Rayleigh (MKS)
Pa	Pascal
s	second
°	degree

Abbreviations:

B & K	Brüel & Kjær
FMBD	flush-mount, bare microphone diaphragm
FMGS	flush-mount grid behind a porous screen
MKS	meter, kilogram, second
NFAC	National Full-scale Aerodynamics Complex
r.m.s.	root mean square
R1.5	1.5-inch microphone recess
SNR	signal-to-noise ratio

TABLE OF FIGURES

Figure 1.1 (a) NASA Ames 40-element array, (b) An acoustically transparent screen covering the microphones	5
Figure 1.2 Ames 31-element array sensor layout	6
Figure 1.3 Preliminary acoustic array background noise test results	6
Figure 2.1 Experimental setup inside the anechoic chamber	16
Figure 2.2 Cut-away view of the quarter-inch diameter B & K microphone	16
Figure 2.3 Experimental setups utilized to simulate both (a) vertical and (b) horizontal components of the 40-element array spiral ...	17
Figure 2.4 Instrumentation flow-chart for the anechoic chamber experiment	17
Figure 2.5 (a) Plastic sleeve, (b) Nylon sleeve, and (c) Rear view of the array panel	18
Figure 2.6 Baseline (Flush-mounted, bare microphone diaphragm) configuration	19
Figure 2.7 Deep recess configuration	19
Figure 2.8 Flush-mount microphone configurations	20
Figure 2.9 Shallow recess microphone configurations	21
Figure 2.10 Typical transfer function data	22
Figure 2.11 Test microphone sound pressure level vs. background level for multiple panel positions	23
Figure 2.12 Reference microphone sound pressure level vs. background level	23
Figure 2.13 Coherence function between test and reference microphones .	23
Figure 3.1 Magnitude and phase for 1 1/2" deep recess foam behind a porous screen test configuration relative to the baseline configuration	32
Figure 3.2 Magnitude and phase for a flush-mounted grid test configuration relative to the baseline configuration	32
Figure 3.3 Magnitude and phase for a flush-mounted grid behind a porous screen relative to the baseline configuration	33

Figure 3.4 Magnitude and phase for protrusion of microphone grid to allow for a flush diaphragm relative to the baseline configuration	33
Figure 3.5 Summary of all flush-mounted configurations presented for incidence angle of zero degrees	34
Figure 3.6 Magnitude and phase for 1.0 mm recess microphone with grid relative to the baseline configuration	34
Figure 3.7 Magnitude and phase for 1.0 mm recess microphone behind a porous screen relative to the baseline configuration	35
Figure 3.8 Magnitude and phase for 1.0 mm bare microphone diaphragm relative to the baseline configuration	35
Figure 3.9 Magnitude and phase for 0.5 mm bare microphone diaphragm relative to the baseline configuration	36
Figure 3.10 Summary of all shallow recess configurations presented for incidence angle of zero degrees	36
Figure 4.1 Power spectrum of the baseline configuration at zero degrees incidence	41
Figure 4.2 Power spectrum of the free field microphone at zero degrees incidence	41
Figure 4.3 Reflection of a plane wave with angle of incidence θ_i and a reflection angle of θ_r at a flat rigid surface	42
Figure 4.4 Sound pressure level increase of array panel which contains a 19- by 19-inch aluminum piece inclusion	42
Figure 5.1 Sound tube (standing wave) apparatus shown with the short tube	48
Figure 5.2 Instrumentation flow-chart for the measurement of acoustic absorption coefficient	48
Figure 5.3 Absorption coefficient as a function of frequency for several sound absorbing material	49
Figure 5.4 (a) Fiberglass sample, (b) Array foam sample, and (c) Combination of array foam and porous screen sample	49

1. INTRODUCTION

Commercial and military aircraft noise has long been an important issue for the aerospace industries both in the United States and around the world. The establishment of stricter regulations on aircraft noise has challenged many aerospace industries to develop quieter engine and airframe components for the next generation of aircraft design, and reduce engine and airframe noise of existing aircraft. Such stringent regulations have increased demands for reliable aeroacoustic measurements in controlled environments, such as wind tunnels, to characterize and reduce sources of aircraft noise. Such measurements require both isolated sensors for acoustic field characterization and multiple-sensor arrays designed to focus on individual noise sources and reject extraneous noise. This is a challenge for airframe noise measurements, since the model generated noise is generally lower than the self-noise of a conventional microphone in a wind tunnel. This paper does not address the self-noise associated with an isolated sensor. The interested reader is referred to references 1 through 4 for more information on the reduction techniques and analysis of microphone self-noise.

Recently, broad band multiple-sensor acoustic arrays have been developed for aeroacoustic measurements of scaled aircraft models in wind tunnels. Typically, a multiple-sensor array for in-flow acoustic measurements contains a pattern of sensors or microphones mounted in a flat, rectangular metal plate which is housed in an aerodynamic fairing. Figure 1.1 shows a 40-element phased microphone array designed and developed at the National Full-scale Aerodynamic Complex (NFAC) and the Information Science Division of NASA Ames Research Center. This array has been utilized during recent airframe noise tests of subsonic and supersonic aircraft models to locate and to characterize noise sources on the models. As can be seen from figure

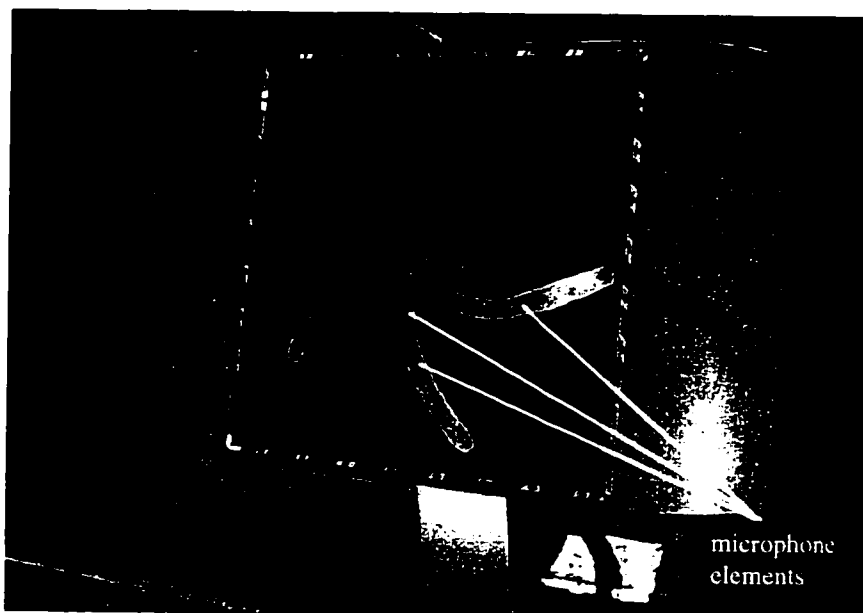
1.1(a), forty microphones are placed within the five spiral arms. The microphones with their protection grids are flush mounted in a flat aluminum plate which is recessed 1.5 inches behind the surface of the fairing. The fairing is supported above the wind tunnel floor by an aerodynamically shaped strut. The material on the front of the fairing, figure 1.1(b), is an acoustically transparent, 100 MKS Rayl stainless steel cloth bonded on a 67% open porous screen. The air gap between the porous screen and the plate is filled with open cell foam with troughs cutout at 45 degrees at the microphone locations. This recessed sensor design was chosen to minimize local turbulent flow noise while maintaining sensitivity to acoustic radiation. The foam served to damp out flow induced vibrations of the porous screen.

In-flow acoustic arrays for wind tunnel research have been developed and applied to aeroacoustic tests for several years at NASA Ames. Early configurations possessed flush-mounted bare microphones diaphragms. In those initial configurations, the leading edge microphones experienced a 10 to 18 dB increase in background noise, which was above the turbulent flow noise measured by a standard microphone aligned with the flow. This is an effect probably due to laminar to turbulent transition occurring at the leading edge sensor locations. This high turbulent flow noise was believed to be a problem for future airframe noise measurement since the sound generated by model scale aircraft is generally near or below the background noise. Consequently, this led to the array developmental study at the Ames 7- by 10-ft wind tunnel to determine a configuration which would effectively minimize flow induced noise near the leading edge microphones.⁵ As seen in figure 1.2, a 31-element microphone array arranged in a cross pattern and mounted in a 34- by 34-inch plate, was utilized during the array developmental study. Only microphone locations 3, 4, 5, 6 and 7 were utilized in the experiment. Figure 1.3 shows the 7- by 10-ft wind tunnel background noise spectrum results acquired by a leading edge sensor (microphone location 3) from three distinct

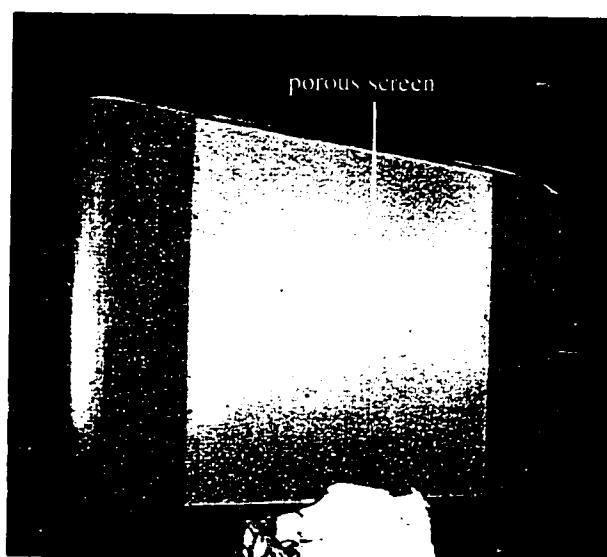
array configurations and are compared with result for an isolated sensor. Tunnel air speed was set at Mach 0.22 for all test runs. As can be seen from the figure, the noise contour obtained from the flush-mount, bare microphone diaphragm (FMBD) shows the worst case result. This configuration reveals a background noise level increase of as much as 16 dB relative to turbulent flow noise (acquired by an isolated sensor) at 5 kHz. This level is, however, decreased to 2 to 3 dB near 20 kHz. Also seen in figure 1.3 is the background noise spectrum for a flush-mount grid behind a porous screen (FMGS) configuration. This level, though larger by several decibels over the level acquired by an isolated sensor, is 2 to 3 dB less than the level acquired by the FMBD configuration in the frequency range up to 20 kHz. A much improved result was obtained by recessing the microphone by 1.5 inches (R1.5) behind a porous screen and filling the immediate air gap around the microphone by an open cell foam, with troughs cut in the foam to expose the microphones. The result obtained from this particular configuration is near or at the level acquired by an isolated sensor for most of the frequency range. In the frequency range of 13 kHz and beyond, the level obtained from this configuration is even lower (by an amount 2 to 3 dB) relative to the level recorded by the same isolated sensor. As a result of the study, the microphone recess behind an acoustically transparent, porous screen was selected for the design of the 40-element array, pictured in figure 1.1.

Because acoustic research at Ames in the future will require array measurements up to 50 kHz or higher, further experimental studies were conducted without flow in the anechoic chamber of NFAC to obtain detailed understanding of the acoustic response due to the various microphone installations over a wide frequency span. The results of these studies are the subject of this thesis. In the first part of this study, since only a limited acoustic assessment was undertaken which suggested some reverberant effects, the experiment was performed to thoroughly document acoustic effects of mounting installation schemes on multiple-sensor arrays used in previous wind tunnel tests.

Subsequently, acoustic studies for extended frequency response in the range of 5 to 50 kHz were conducted for other various microphone installations to identify configurations with favorable magnitude and phase response to an external source. Also included in this thesis are theoretical and experimental results from an anechoic chamber test conducted to assess the response of the microphone mounted in a flat plate relative to the same microphone isolated in free field at the same location. Theoretical and experimental results are also presented for a sound tube test conducted to measure sound energy absorption coefficient of an open foam sample (same foam used on the Ames 40-element microphone array), a porous screen sample, the combination of an open foam sample and a porous screen sample, and a fiberglass sample (material is used to cover floor grating of Ames anechoic chamber).



(a)



(b)

Figure 1.1 (a) NASA Ames 40-element array
(b) An acoustically transparent screen covering the microphones

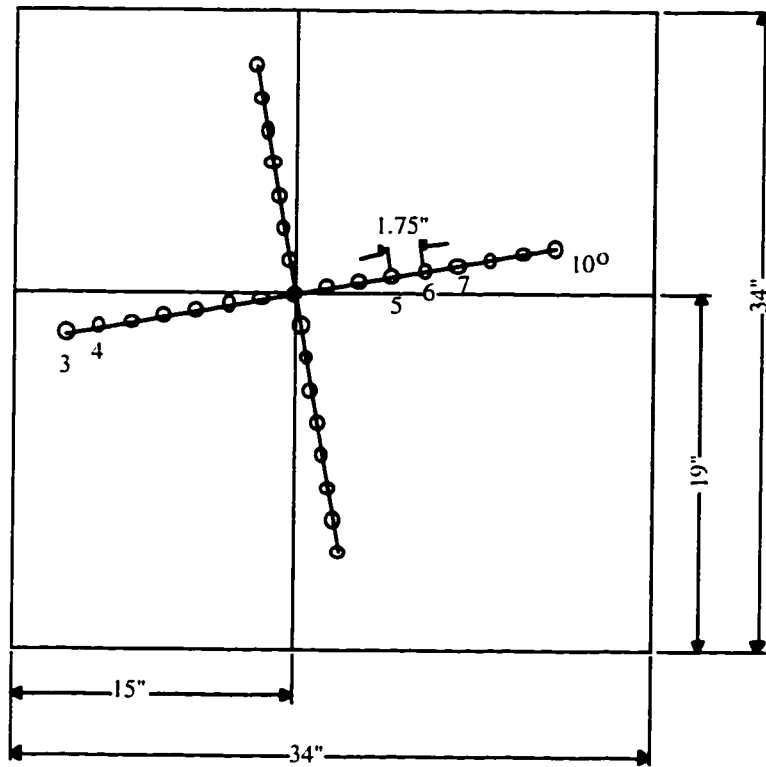


Figure 1.2 Ames 31-element array sensor layout

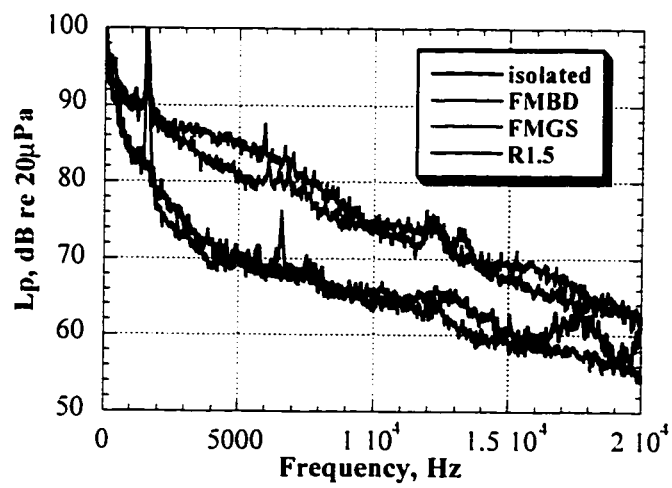


Figure 1.3 Preliminary acoustic array background noise test results

2. EXPERIMENTAL APPROACH

The experiment was conducted in the anechoic chamber at NASA Ames Research Center. The anechoic chamber has free space of 25- by 18- by 11-feet and is anechoic to sound frequencies greater than 150 Hz.

2.1 Test Setup and Instrumentation

To investigate its response, the microphone panel under study included placement of a single (test) microphone in the center of a 48- by 48- by 0.25-inch masonite panel. This material was selected because of its capability to simulate an almost perfectly sound reflecting surface as with an actual array surface. The size was selected to correspond to the size of the wind tunnel array. The frontal (planar) dimensions of the panel were several wavelengths larger than the largest wavelength evaluated, which was approximately 2 inches at the lowest test frequency of 5 kHz. The edges were also far enough from the test microphone to minimize edge scattering effects onto the test microphone. Figure 2.1 is a photograph of the experimental setup.

A second (reference) microphone was placed in free space away from the panel and pointed at the source. The placement of the reference microphone in this experiment was chosen such that it met the following conditions:

1. The reference microphone is close enough to the test microphone so that the coherence function between the two microphones is high. This high coherence is required for the signal processing method selected for this experiment.

2. The reference microphone is placed far enough from other test hardware so that it is unaffected by reflections.
3. The reference microphone's position and orientation do not change throughout the course of the experiment.
4. The reference microphone is pointed directly at the source. This condition provides the highest signal response at high frequencies and thus maximizes the signal-to-noise ratio across the reference microphone's frequency range.
5. Both microphones are positioned at a fixed radial distance of 12 feet from the source.

The reference microphone's position was 34 inches below the test microphone, 17 inches to the side of it, and 6 inches in front of it. The placement of the reference microphone in this fashion meets all five conditions discussed above. The source was positioned at the same height as the test microphone, 5.5 feet above the anechoic chamber floor. The floor gratings in figure 2.1 were covered with sound absorbing fiberglass to prevent source reflections from contaminating the measurements. The noise source used in this experiment was compact and produced an adequate signal-to-noise ratio (SNR) in the frequency range of 5-50 kHz.

Brüel & Kjær (B & K) type 4135 1/4-inch condenser microphones were selected for both the test and the reference sensors. As can be seen on the cut-away view of figure 2.2 (figure is obtained from the Brüel & Kjær data handbook in reference 6), the B & K type 4135 condenser microphone has a main body housing of monel, on which a thin (on the order of 1.5 μm) nickel diaphragm is mounted.⁶ Condenser microphones employ a diaphragm as one side of a capacitor and when the diaphragm deflects due to a change in sound pressure, the resulting change in capacitance is converted to an electrical signal.

Quarter-inch-diameter B & K condenser microphones were selected for this experiment because of their accuracy, frequency characteristics, long term stability and insensitivity to changes in ambient conditions. Also shown in figure 2.2 is a microphone diaphragm protection grid. Protection grids are used to protect microphone diaphragms from damage by contact with other objects. Protection grids are also fitted around bare microphone diaphragms for all pistonphone calibrations. Several test configurations in this experiment utilized the protection grid fitted around the microphone diaphragm.

Figure 2.3(a) and 2.3(b) shows experimental setups utilized to determine the acoustic effects of mounting installation schemes on the microphone recess behind a transparent, porous screen configuration. Since only a limited acoustic assessment of this configuration was undertaken which suggested some reverberant effects, the acoustic effects of the installation were more thoroughly studied in the present investigation. The test microphone, fitted with its protection grid, was recessed at 1.5 inches behind a 67% open porous screen covered with 100 MKS Rayl stainless steel cloth. A 34- by 18- by 1.5-inch open cell foam insert was used to fill the immediate air gap between the porous screen and the array panel near the test microphone. This was the mounting arrangement employed in recent test applications of the 40-element array in the 40- by 80-ft wind tunnel at Ames. A 26- by 2-inch trough at 45 degrees was cut to allow the penetration of acoustic waves at the test microphone location. The open cell foam in this experiment was tested at both the vertical (figure 2.3(a)) and at horizontal (figure 2.3(b)) orientations. Since the troughs on the five spiral arms of the 40 element array (seen on figure 1.1(a)) are situated in a multi-dimensional plane, i. e., a 2-dimensional plane, the above setups will simulate both a vertical and a horizontal component of the spiral.

Figure 2.4 is an instrumentation diagram for the anechoic chamber study. The white noise input signal to the speaker was supplied with a random noise generator. The output signals from the test and the reference microphones were connected to a dynamic

signal analyzer and a digital oscilloscope for analysis and display. All data were analyzed using 100 averages and a resolution bandwidth of 125 Hz.

2.2 Apparatus Construction and Mounting

Throughout the experiment, the test microphone was mounted in a 0.25-inch-thick masonite panel bonded to a 1-3/4-inch-thick plywood base. As seen in figure 2.5, the test microphone was first placed either through a white plastic sleeve (inside diameter ≈ 7.5 mm) or through a nylon sleeve (inside diameter $D \approx 6$ mm) and the assembly was then secured in the center of the panel. Those test configurations which required utilization of the microphone protection grid used the white plastic sleeve and those test arrangements which required a bare microphone diaphragm configuration used the nylon sleeve (the nylon sleeve was obtained from Boeing and was slightly modified in this experiment). The reference microphone was fastened on a right angle adapter extension arm.

Figures 2.6 through 2.9 show experimental configurations discussed in this paper. Figure 2.6 shows a flush-mount, bare microphone diaphragm configuration (baseline configuration). Figure 2.7 shows the Ames existing installation scheme (deep recess configuration). The microphone and its protection grid is recessed 1.5 inches behind a porous screen. The immediate air gap around the microphone is filled with open cell foam. Figure 2.8 shows flush-mount configurations and figure 2.9 shows shallow recess configurations. All of the installation configurations just described are related to the baseline configuration. This relation is discussed in detail in the next section.

2.3 Analysis Method

The first step in the study was to select a baseline configuration to which all other configurations are related. Figure 2.6 shows a cut-away view of the baseline configuration. The test microphone was mounted flush with the array surface and possessed no protection grid.

To determine the response of a microphone mounted in a microphone panel, it was necessary to take separate measurements of the baseline configuration and the installation configuration. The measurements were then related, via the reference microphone, to determine the various installation effects. The acoustic differences between microphone installation configurations are determined by measuring the complex transfer function (magnitude expressed in decibel and phase expressed in degrees) between the test microphone in each installation configuration and the reference microphone. The decibel (abbreviated dB) is a dimensionless unit for expressing the ratio of two powers, which can be acoustical, mechanical, or electrical, and the number of decibels is 10 times the logarithm to the base 10 of the power ratio. The ratio between the transfer functions of the two different configurations (baseline and installation) results in the transfer function between the two different configurations since the reference microphone information cancels itself. The method used for calculating the magnitude and phase of the transfer function between two microphone signals (test and reference) with a common input was the cross-spectrum method.⁷

This method takes the cross-spectrum of a two sensor measurement and calculates the transfer function as

$$H(f) = \frac{G_{xy}(f)}{G_{xx}(f)} = \frac{G_{(ref)(test)}(f)}{G_{(ref)}(f)} \quad (1)$$

where $H(f)$ represents the transfer function, $G_{xy}(f)$ represents the cross-spectrum measurement between the reference and test microphone channels and $G_{xx}(f)$ represents the power spectrum of the reference microphone. This method is very accurate since it eliminates uncorrelated noise at the microphones.

For a typical test configuration and acoustic incidence angle the transfer function of the baseline configuration relative to the fixed reference microphone was measured as $H(f)_{\frac{baseline}{ref}}$ on a signal analyzer. Then, for the same incidence angle, the transfer function of the installation configuration relative to the fixed reference microphone was measured as $H(f)_{\frac{installation}{ref}}$ on the signal analyzer. Once the two set of measurements were completed, the transfer function of the installation configuration relative to the transfer function of the baseline configuration was formed as the ratio

$$H(f)_{\frac{installation}{baseline}} = \frac{H(f)_{\frac{installation}{ref}}}{H(f)_{\frac{baseline}{ref}}} \quad (2)$$

Note that the reference conditions from the previous equation have dropped out, leaving only the installation effects relative to the baseline configuration.

Figure 2.10 shows a typical result. This result was formed as the ratio of the two previous measurements presented in figures 2.10(a) and 2.10(b). Figure 2.10(a) shows the transfer function of the baseline configuration as $H(f)_{\frac{baseline}{ref}}$. This figure provides information for both the magnitude and the phase portions from the transfer function.

Similarly, figure 2.10(b) shows both the magnitude and the phase portions from the transfer function for a typical installation configuration as $H(f)_{\frac{installation}{ref}}$. Figure 2.10(c), therefore, presents the final result for a typical installation configuration. This result is formed as the ratio of the transfer function of the installation configuration with respect to the transfer function of the baseline configuration as $H(f)_{\frac{installation}{baseline}}$.

Signal-to-noise ratio consideration - Figures 2.11 and 2.12 show samples of both the test and the reference microphone power spectrums and their corresponding background levels in the frequency range 125 Hz to 50 kHz. The test microphone was flush mounted in the array and possessed no protective grid (baseline configuration). As can be seen from figure 2.11 the test microphone for the array panel positions of 0, 30, and 60 degrees displays a 55 dB signal over the background level in the mid frequency range (5 to 25 kHz). The test microphone for array position of 90 degrees shows a 48 dB signal over the background level in the same frequency range. The signal to noise ratio for array positions of 0 and 30 degrees are 33 dB and 25 dB, respectively, at 50 kHz. The signal to noise ratio for array positions of 60 and 90 degrees are about 15 dB at 50 kHz. For the purpose of this experiment, a 15 dB signal to noise ratio was deemed adequate.

The reference microphone's power spectrum is shown on figure 2.12. Four separate measurements were taken and compared here as the array panel was rotated from 0 to 90 degrees in increments of 30 degrees. The three curves for array panel positions of 0, 30, and 90 degrees can be seen to exhibit just about the same response. The signal to noise ratio for all four measurements is about 50 dB from low to mid frequencies and 20 dB at 50 kHz. From the above observations, it is seen that the signal to noise ratio was acceptable for both microphones across the entire frequency range.

2.4 Measurement Accuracy and Experimental Error

Reference 7 points out two sources of error that occur in the analysis of random data, termed random and bias errors. Random errors in estimating frequency response functions are due to the measurement noise in the transducers and instrumentation, and computational noise in the digital calculations. The resulting random error due to these sources is directly related to the coherence function $\gamma_{xy}^2(f)$ calculated between the two microphones, and the number of averages n_d . The measurements in this experiment were each averaged for 100 blocks and at a frequency resolution bandwidth of 125 Hz.

Figure 2.13 shows the coherence function between the test and the reference microphones for array panel positions of 0, 30, 60, and 90 degrees of incidence angle with the source. The test microphone is mounted flush with the array surface and the reference microphone's position is unchanged. As can be seen from the figure, the coherence between the two microphone is about 0.97 for the frequency range of interest from 5 - 50 kHz. For the array panel position of 60 degrees, it is seen that the coherence function drops off slightly to about 0.95 from about 5 to 24 kHz. From equation (5.52) of reference 7, a coherence of 0.95 will produce a normalized random error in the estimated gain factor and a standard deviation in the estimated phase factor of 1.6% and 0.93 degrees, respectively. These value are well within the desired accuracy of the measurements.

The other source of error that is mentioned in reference 7 in random data is the bias error. It is a systematic error that will appear with the same magnitude and in the same direction from one data analysis to the next. Early on in the study, it was observed that a very slight displacement or bending of the array panel under certain weight, i. e., the porous screen weight, between the two sets of measurements (baseline and a test

configuration) caused a significant shift on the phase portion of the transfer function. The effects in the magnitude portion were negligible. The porous screen which has the same planar dimensions as the array panel imposed a non-elastic bend on the array panel itself. It was shown that a very slight linear displacement of the array panel from its original position caused a phase shift of more than 10 degrees. A phase shift of more than 10 degrees was outside the desired accuracy range. As a result the 0.25-inch panel was secured on a 1 and 3/4-inch-thick plywood to keep it from being displaced. The difference was readily apparent and the linear phase shift was, as a result, brought to within the desired phase accuracy range of ± 10 degrees over the 50 kHz bandwidth.

One other source that introduced apparent error into the measurements (due to differences in wave propagation speed between the two paths) was a temperature drift that occurred in between the two sets of measurements. For instance, a half degree Fahrenheit change in temperature resulted in 104 degrees of phase shift at 50 kHz. In order to account for this, the two microphones, as discussed in *Test Setup and Instrumentation* section, were positioned at a constant radial distance from the source to ensure that the propagation delay was the same for the two sensors.

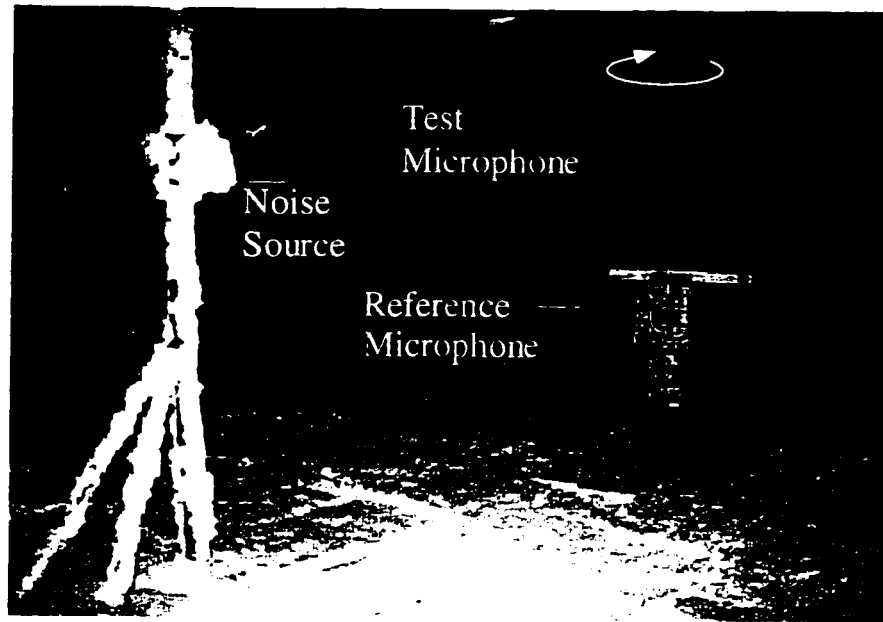
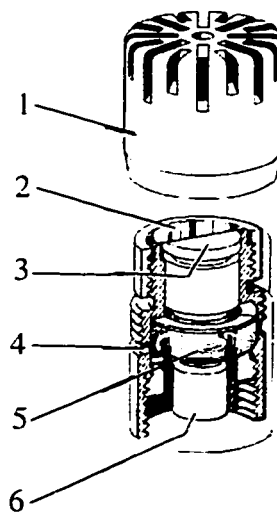


Figure 2.1 Experimental setup inside the anechoic chamber



1. Protection grid
2. Diaphragm
3. Backplate
4. Static pressure equalization ventilation
5. Insulator
6. Output terminal

Figure 2.2 Cut-away view of the quarter-inch diameter Brüel & Kjær microphone

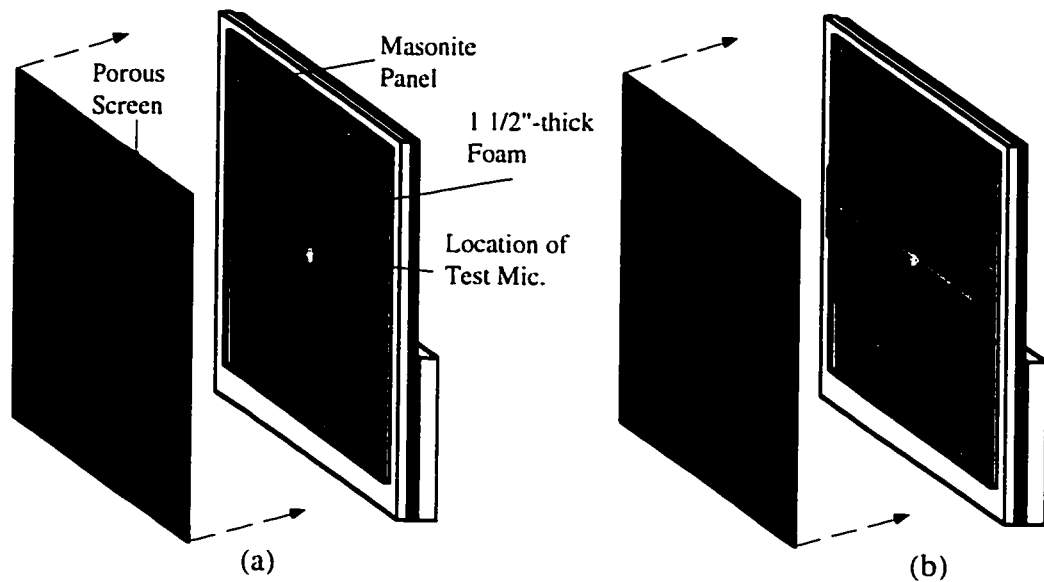


Figure 2.3 Experimental setups utilized to simulate both (a) vertical and (b) horizontal components of the 40-element array spiral

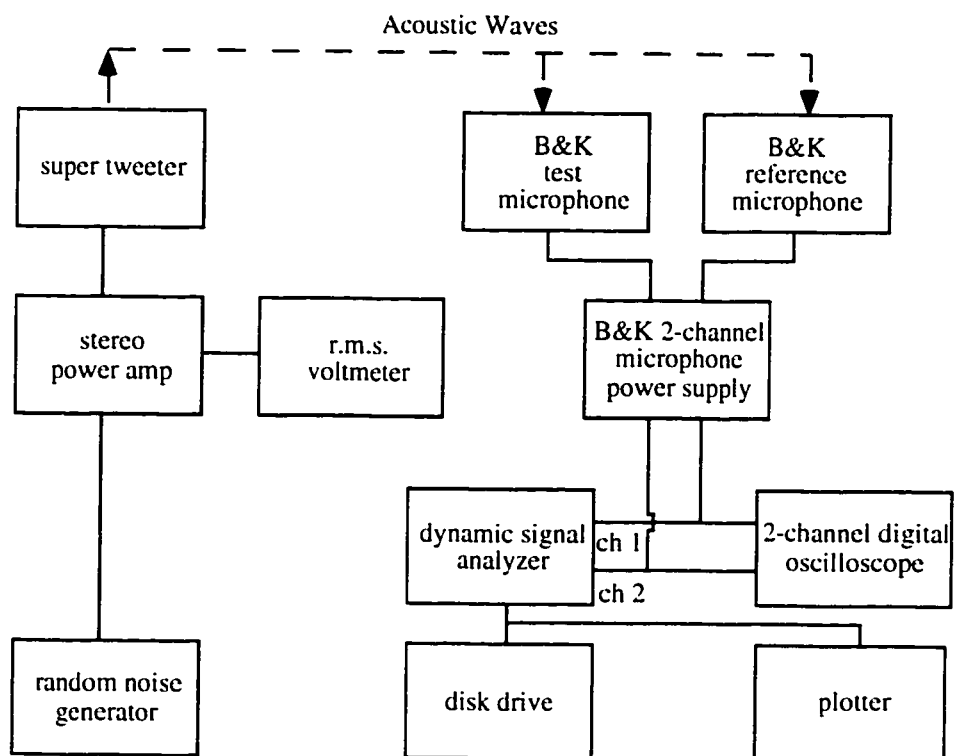


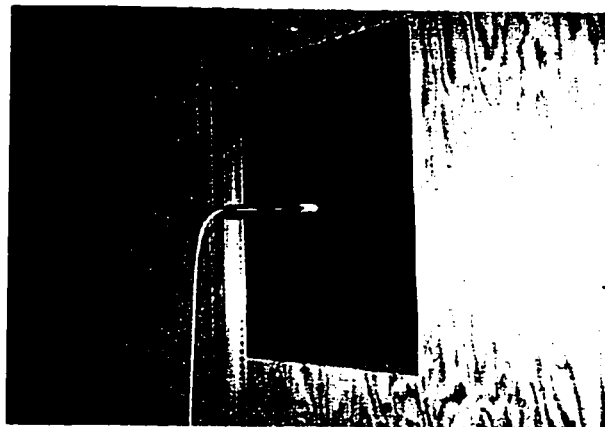
Figure 2.4 Instrumentation flow-chart for the anechoic chamber experiment



(a)

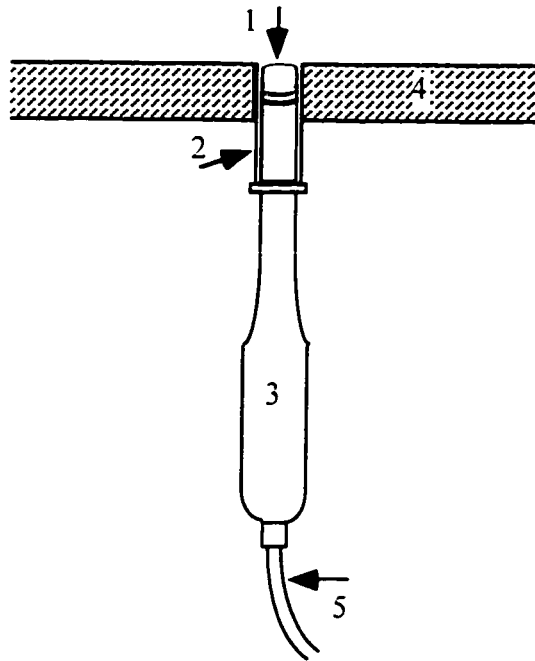


(b)



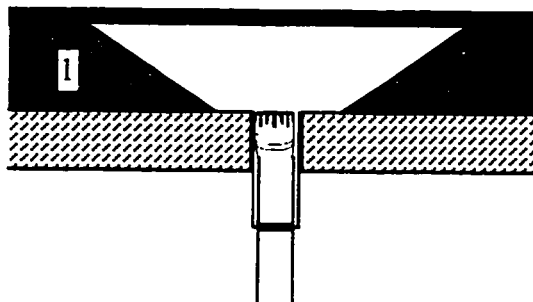
(c)

Figure 2.5 (a) Plastic sleeve
(b) Nylon sleeve
(c) Rear view of the array panel



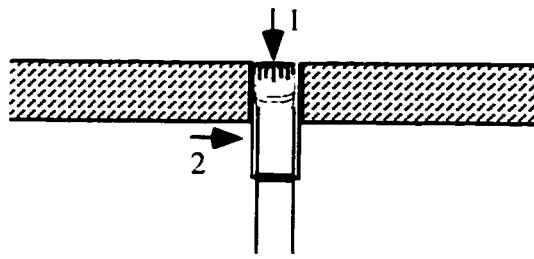
- | | |
|------------------------------|---------------------------|
| 1. Bare microphone diaphragm | 4. Array panel (masonite) |
| 2. Nylon sleeve | 5. Microphone cable |
| 3. Microphone preamp | |

Figure 2.6 Baseline (Flush-mounted, bare microphone diaphragm) configuration

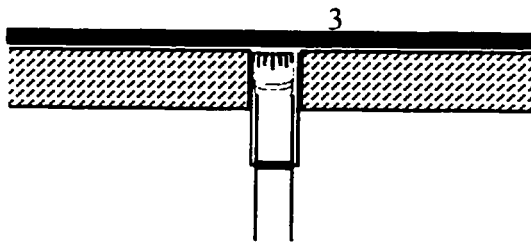


1. 1 1/2"-thick foam

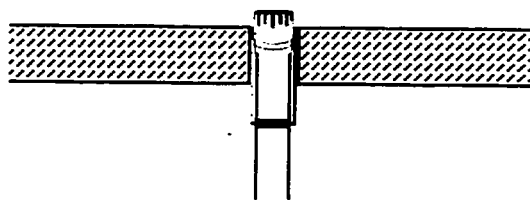
Figure 2.7 Deep recess configuration



(a) Flush-mounted grid



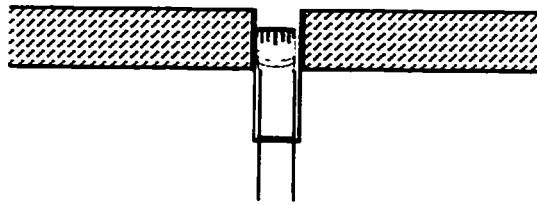
(b) Flush-mounted grid behind porous screen



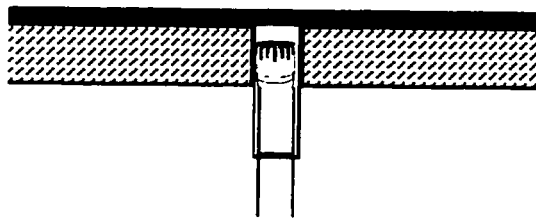
(c) Protrusion of mic grid to allow flush diaphragm

1. Microphone protection grid
2. Plastic sleeve
3. 100 MKS rayl stainless steel cloth bonded on 68-% open porous screen

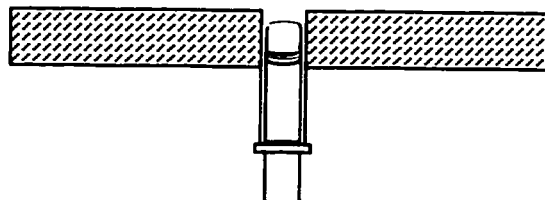
Figure 2.8 Flush-mount microphone configurations



(a) 1 mm recess microphone with protection grid



(b) 1 mm recess mic with grid behind porous screen



(c) 1 mm recess bare microphone diaphragm

Figure 2.9 Shallow recess microphone configurations

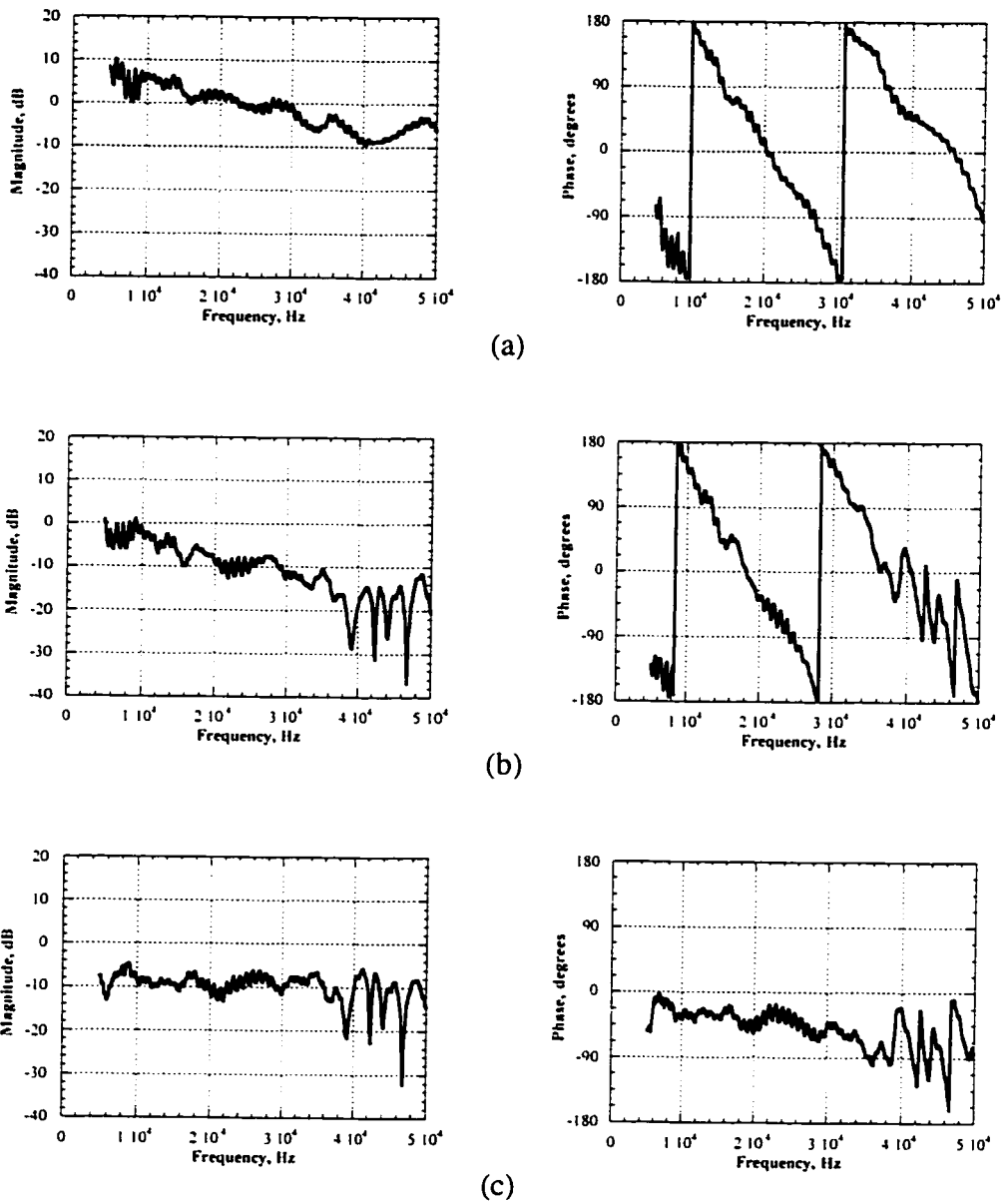


Figure 2.10 Typical transfer function data

- (a) Magnitude and phase from the transfer function of the baseline configuration
- (b) Magnitude and phase from the transfer function of the installation configuration
- (c) Ratio of the transfer function of the installation configuration with respect to the transfer function of the baseline configuration

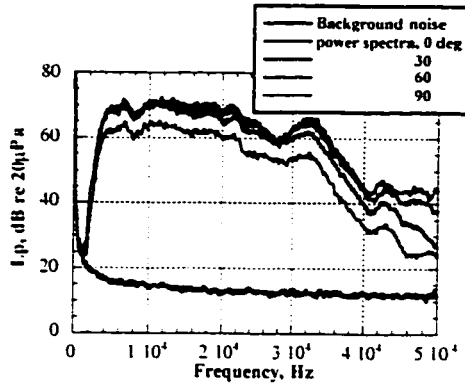


Figure 2.11 Test microphone sound pressure level vs. background level for multiple panel positions

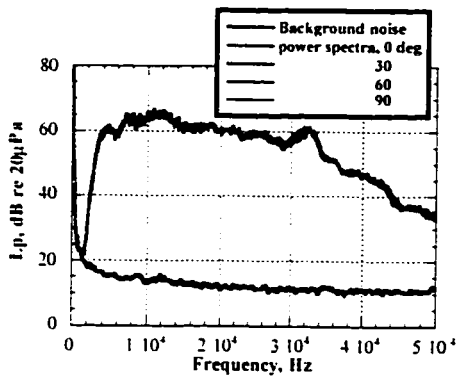


Figure 2.12 Reference microphone sound pressure level vs. background level

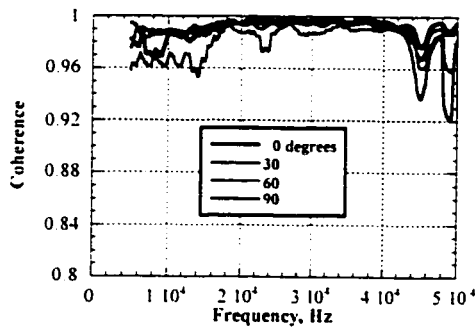


Figure 2.13 Coherence function between the test and the reference microphones

3. RESULTS AND DISCUSSION

The B & K type 4135 condenser microphone is normally fitted with a protection grid which is also required for pistonphone calibration. This and the next section will present results for several configuration cases where the protection grid was used in the flat plate installation. The B & K protection grid and microphone diaphragm form an open cavity and are 1 mm (0.03937 in) apart.

It should be noted that a few of the figures in the following sections may show random noise in the data traces. Random noise will be especially apparent for larger panel angular positions. This is an effect due to the loss in the signal-to-noise ratio, as discussed in section 2.3. The test microphone in this experiment exhibited lower signal response at larger panel angular positions. It showed the highest signal responses when the noise source impinged on the microphone diaphragm at zero degrees incidence.

3.1 Effects of Deep Recess Configuration

Figure 3.1 shows magnitude and phase results from the transfer function for the experimental setups of figure 2.3 and 2.7. Data seen as the black solid line presents results for the vertical foam channel and the porous screen configuration while data seen as the red solid line presents results for the horizontal foam channel and the porous screen configuration. Results in both experimental cases indicate poor installation configurations with unacceptably large amplitude and phase oscillations. Results in figure 3.1 show degradation, relative to a flush-mounted bare diaphragm baseline configuration, as much as 8.5 dB peak-to-peak in magnitude at 36 kHz (vertical foam channel) and 8 dB peak-to-peak in magnitude at 35 kHz (horizontal foam channel).

Phase oscillations, as much as 90 degrees peak-to-peak, are also seen for both experimental setups.

Horne, Hamid, and Cooper witnessed similar reverberant effects during a multiple parabolic reflector calibration in the anechoic chamber when the same porous screen covering was used to cover the reflector.⁸ Variations of about 2 dB peak-to-peak magnitude was measured with the inclusion of the porous screen in this study.

3.2 Effects of Flush-Mount Configuration

3.2.1 Flush-mounted Microphone Protection Grid Configuration

Figure 3.2 shows magnitude and phase portions of the transfer function for a flush-mounted grid test configuration in the frequency range 5 to 50 kHz. Data on this figure is presented for panel positions of 0, 30, 45 and 90 degrees of incidence angle with the source. A sketch of this test configuration can be seen in figure 2.8(a). Deviations from a flat transfer function are apparent for both the magnitude and phase in this test configuration. The general shape of the transfer function shows increased oscillating amplitudes, but decreasing phase with respect to the frequency. As can be seen from the same figure, the transfer function shows three major oscillations in the amplitude and phase of the transfer function. Oscillations in the amplitude and phase portions from the transfer function occur near 8, 28 and 40 kHz for all four panel positions. These oscillations range as much as 6 dB peak-to-peak in magnitude and -30 degrees in phase near 8 kHz in all four panel rotations. Oscillations near 28 kHz can be seen to extend to almost -8 dB (for 60 degree panel position) in amplitude and -60 degrees in phase. Near 40 kHz, all four traces, both magnitude and phase, are further laid apart from each other

than the lower frequency ranges. Note, the small levels of random noise in the data, as described above, pertains to the array position of 90 degrees near 40 kHz and beyond.

3.2.2 Flush-mounted Grid behind Porous Screen

Figure 3.3 shows both the magnitude and phase portions of the transfer function for a flush-mounted grid behind a porous screen test configuration in the frequency range 5 to 50 kHz. Data on this figure is presented for panel positions of 0, 30, and 60 degrees of incidence angle with the source. A sketch of this test configuration can be seen in figure 2.8(b). The porous screen and the grid were closely spaced in this test configuration. Deviations from a flat transfer function are apparent for both the magnitude and phase in this test configuration. The general shape of the transfer function at panel angular positions of 0 and 30 degrees shows results that are similar to the results obtained for a flush-mounted microphone with a protection grid configuration. The magnitude portion from the transfer function is shown to oscillate about the 0-dB line on the ordinate of figure 3.3. High frequency oscillations, as a result of mounting the porous screen, are also vivid for these two positions in the lower frequency ranges, from about 5 to 20 kHz. For array position of 60 degrees, the data trace for the magnitude portion of the transfer function also shows high frequency oscillations from about 5 to 38 kHz. The data trace for the same array position beyond 38 kHz shows two resonances, one at about 43 kHz and the other at 45 kHz.

The general shape of the phase portion of the transfer function shows decreasing phase angles with respect to the frequency. One resonance near 8 kHz for all three array positions is apparent. Note the high frequency oscillations of data traces as a result of the porous screen cover for array positions of 0 and 30 degrees from about 5 to 20 kHz.

3.2.3 Protrusion of Microphone Grid to Allow Flush Diaphragm

During this test sequence, the microphone protection grid was protruded 1.5 mm (1 mm cavity gap between the diaphragm and the protection grid plus 0.5 mm protection grid thickness) to allow a flush-mounted diaphragm. Results for panel positions of 0, 45, 60 and 90 degrees of incidence angle with the source are presented in figure 3.4. Experimental setup is shown in figure 2.8(c). Deviation from a flat transfer function is readily apparent for the magnitude portion. The general shape of the magnitude portion of figure 3.4 shows increasing amplitudes from about 5 to 40 kHz, but then shows decreasing amplitudes beyond 40 kHz. The four traces are somewhat apart in this latter frequency range. Two resonances, one near 8 kHz and the other near 25 kHz, occur for all panel positions, except for array position of 90 degrees incidence with the source. This latter position exhibits noise in the data trace beyond 40 kHz.

The general shape of the phase portion of the transfer function in figure 3.4 shows relatively smooth phase angles for all four panel positions with respect to the 0-dB line from about 5 to 40 kHz, but the four curves then drop to -60 degrees of phase angles beyond 40 kHz.

Figure 3.5 summarizes test results for the above three test configurations. Please refer back to figure 2.8 for graphical descriptions of all flush-mount configurations. Results are presented here for comparison and discussion purposes for the panel position of zero degrees incidence with the source only. As can be seen from the figure, all three test setups show poor installation results. All three curves show large oscillations about the 0-dB line in figure 3.5. These oscillations are as much as 6 dB peak-to-peak in magnitude. The data for the flush-mounted grid behind the porous screen, seen as the red

solid line in figure 3.5, not only shows large oscillations in the frequency range, it also displays high frequency reverberation effects from about 5 to 20 kHz. These high frequency reverberations for the same test setup is also seen in the phase of the transfer function, also in the same frequency range.

Results for the next section will include all shallow recess configurations. The results for the first two sub-sections include results with the use of the microphone protection grid. The last sub-section includes results without the use of the microphone protection grid. A summary and discussion of all three shallow recess configurations will be presented at the end of section 3.3.3.

3.3 Effects of Shallow Recess Configurations

3.3.1 1 mm Recess Microphone with Protection Grid

Figure 3.6 presents results for the 1 mm recess microphone grid test configuration. This recess length plus the 1 mm cavity gap between the test microphone diaphragm and the protection grid places the diaphragm 2 mm behind the surface of the array panel. Data in this figure is presented for panel positions of 0, 30, and 60 degrees of incidence angle with the source. Experimental setup is shown in figure 2.9(a). Deviations from a flat transfer function are apparent for both the magnitude and phase with respect to the frequency. Data presented for this test configuration looks similar in shape to the data from the flush-mounted grid behind the porous screen test configuration of section 3.2.2. The general shape of the magnitude portion of the transfer function at all three array panel orientations shows oscillations about the 0-dB line in figure 3.6 in the frequency range about 8 to 40 kHz. Beyond 40 kHz, data does not show any

oscillations anymore, except for array position of 60 degrees. Random noise can be seen to be an inherent part of almost all test configurations at this incidence angle with the source.

The general shape of the phase portion of the transfer function shows decreasing phase angle with respect to the frequency. Two resonances, one near 8 kHz and the other near 29 kHz, occur in the data traces.

3.3.2 1 mm Recess Microphone with Grid behind Porous Screen

Data presented in figure 3.7 shows results for the 1 mm recess microphone protection grid behind the porous screen in the frequency range 5 to 50 kHz. Data were obtained for panel positions of 0, 30, and 60 degrees incidence angle with the source. Experimental setup is shown in figure 2.9(b). Data presented in this sub-section looks largely similar to data obtained for the 1 mm recess microphone with protection grid of section 3.3.1. Namely, data traces for the magnitude portion from the transfer function exhibit oscillations from about 8 to 50 kHz for panel positions of 0 and 30 degrees incidence with the source. Note, the small levels of noise in the data (described above) also pertains for the panel position of 60 degrees incidence with the source. The inclusion of the porous screen has also included high frequency reverberation for the panel positions of 0 and 30 degrees in the frequency range 5 to about 20 kHz. This is consistent with the results obtained for the flush-mount microphone protection grid behind the porous screen test configuration of previous section.

The general shape of the phase portion of the transfer function shows decreasing phase angle with respect to the frequency. Again, data presented here largely imitate

results obtained earlier in the previous section. Two resonances, one near 8 kHz and the other near 28 kHz, occur for all array incidence angle with the source.

3.3.3 1 mm Recess, Bare Microphone Diaphragm

Figure 3.8 shows magnitude and phase portions of the transfer function for a 1 mm recess, bare microphone diaphragm test configuration in the frequency range 5 to 50 kHz. Data on this figure is presented for panel positions of 0, 30, 45, and 60 degrees of incidence angle with the source. Graphical setup of this test configuration can be seen in figure 2.9(c). The results, both magnitude and phase from the transfer function, for this test configuration so far show improved results with relatively smooth amplitude and phase. In the frequency range from 5 to about 13 kHz, the transfer function shows no major changes in current test configuration with respect to the flush-mount bare microphone baseline configuration. In the frequency range between 13 and 20 kHz, the magnitude portion from the transfer function increases by about 3 dB for all panel incidence positions with the source. Beyond 20 kHz, the curves remain relatively constant with frequency, except for the panel position of 60 degrees where random noise variations are present. The phase portion from the transfer function beyond 20 kHz for all panel positions are seen to decrease to about -65 degrees at 50 kHz. High noise levels for panel position of 60 degrees are also present in this figure.

At the end of this setup, the panel was rotated back to zero degrees of incidence angle with respect to the noise source. The test microphone was shifted forward by approximately 0.5 mm from the 1 mm recess position. This setup was performed in attempt to determine the response of the panel as the test microphone is brought closer to a flush mount. This setup was tested at zero degrees incidence angle with the source

only. Figure 3.9 shows both magnitude and phase portions from the transfer function. As can be seen, this configuration has the most regular magnitude and phase response to an external source as the bare microphone diaphragm is placed near a flush mount.

Figure 3.10 summarizes test results for the above four test configurations. Please refer back to figure 2.9 for graphical descriptions of all test setups. Results are presented here for comparison and discussion purposes for the panel position of zero degrees incidence angle with the source only. As can be seen from the figure, the first two installation configurations (1 mm recess microphone grid and 1 mm recess microphone grid behind the porous screen) show worst of the four data results. They show a ± 5 dB oscillations in magnitude about the 0-dB line with respect to the frequency. The 1 mm recess microphone grid behind the porous screen also exhibits high frequent reverberations from 5 to 20 kHz, in both magnitude and phase from the transfer function. The 1 mm recess, bare microphone diaphragm (data seen as solid green line) shows improved results with relatively smooth amplitude and phase. The transfer function shows no major changes in this test configuration with respect to the flush-mounted bare microphone baseline configuration. In the frequency range of 20 to 50 kHz, there is a constant increase in magnitude of about 3 dB.

The data for the 0.5 mm test configuration at the panel position of zero degrees with source shows the best results obtained in this experiment. The shape of the transfer function shows the most regular magnitude and phase response to the noise source. The results from this configuration suggests that the magnitude and phase from the transfer function will approach a flat or ideal response as the test microphone diaphragm is placed near a flush mount.

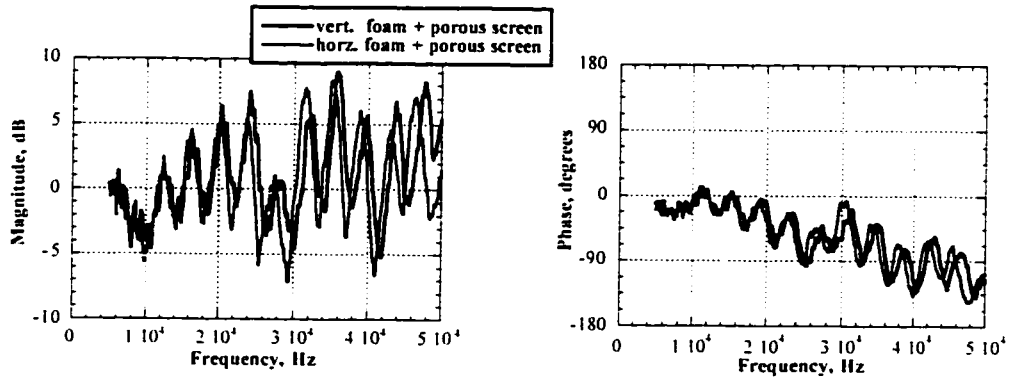


Figure 3.1 Magnitude and phase for 1 1/2" deep recess foam behind a porous screen test configuration relative to the baseline configuration

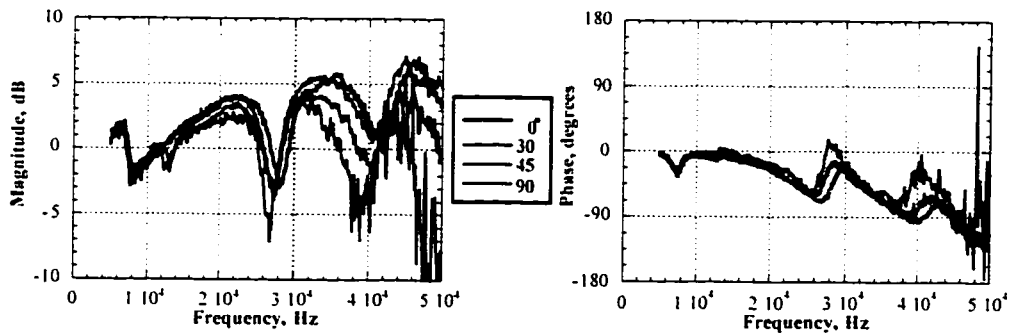


Figure 3.2 Magnitude and phase for a flush-mounted grid test configuration relative to the baseline configuration

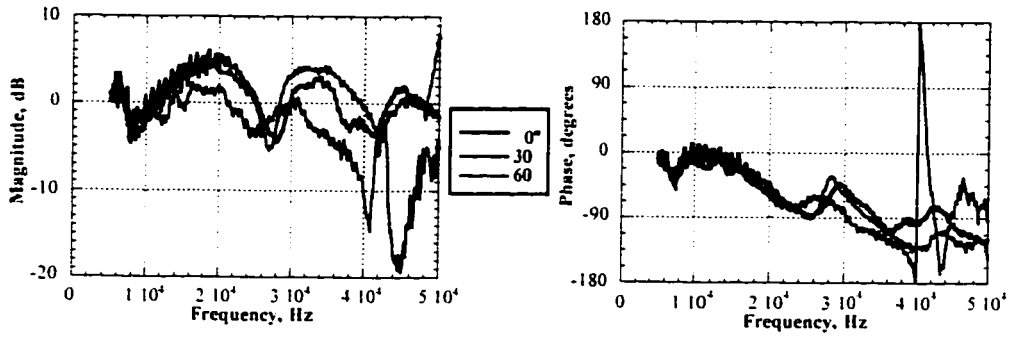


Figure 3.3 Magnitude and phase for a flush-mounted grid behind a porous screen relative to the baseline configuration

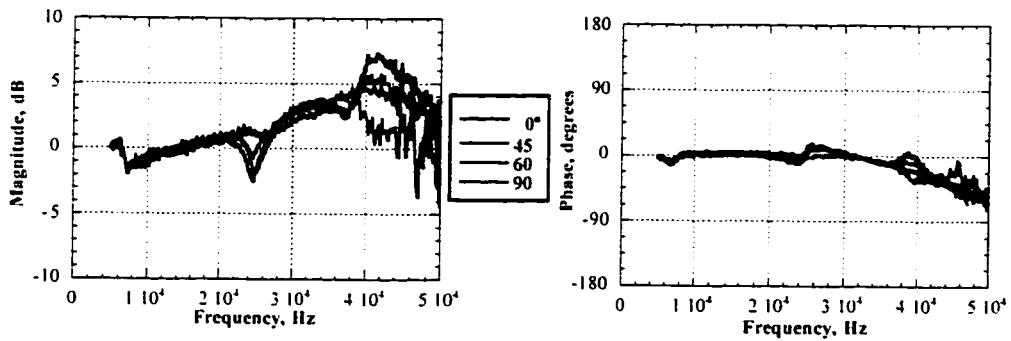


Figure 3.4 Magnitude and phase for protrusion of microphone grid to allow for a flush diaphragm relative to the baseline configuration

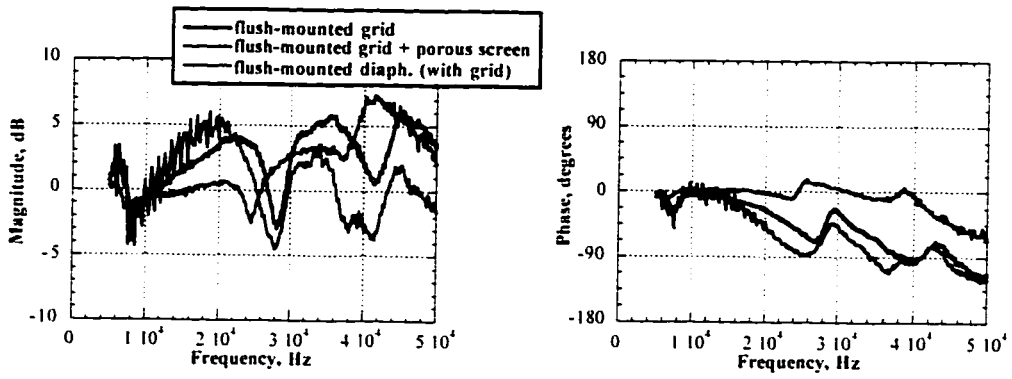


Figure 3.5 Summary of all flush-mounted configurations presented for incidence angle of zero degrees

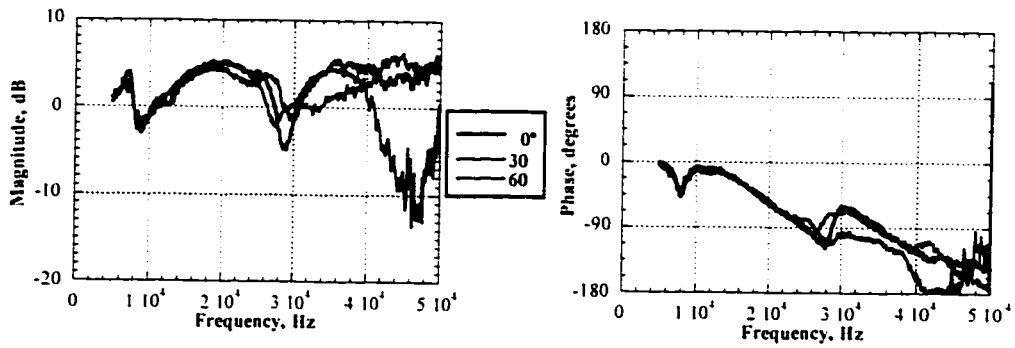


Figure 3.6 Magnitude and phase for 1.0 mm recess microphone with grid relative to the baseline configuration

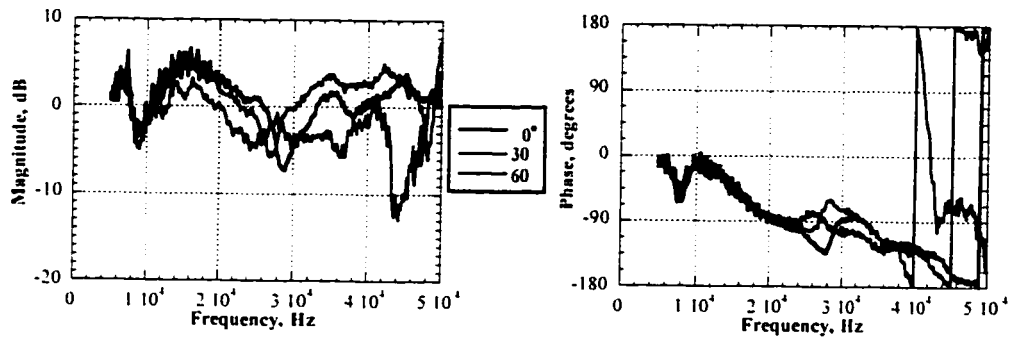


Figure 3.7 Magnitude and phase for 1.0 mm recess microphone behind a porous screen relative to the baseline configuration

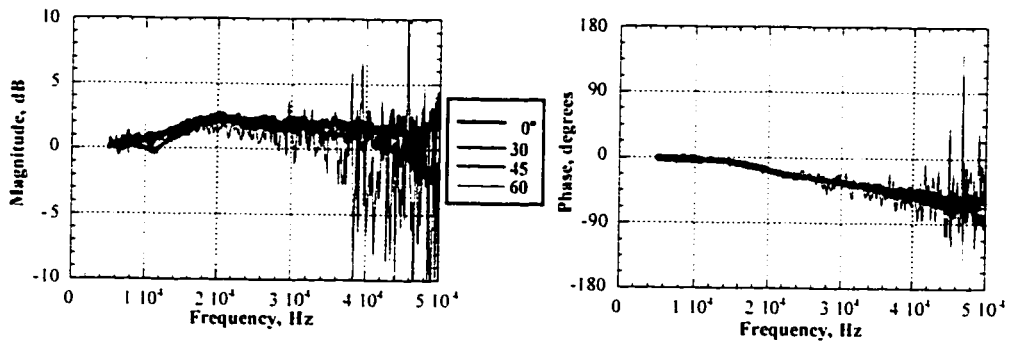


Figure 3.8 Magnitude and phase for 1.0 mm bare microphone diaphragm relative to the baseline configuration

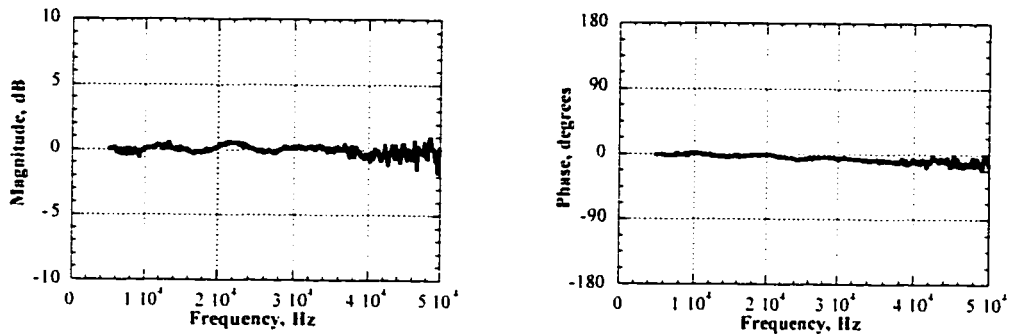


Figure 3.9 Magnitude and phase for 0.5 mm bare microphone diaphragm relative to the baseline configuration

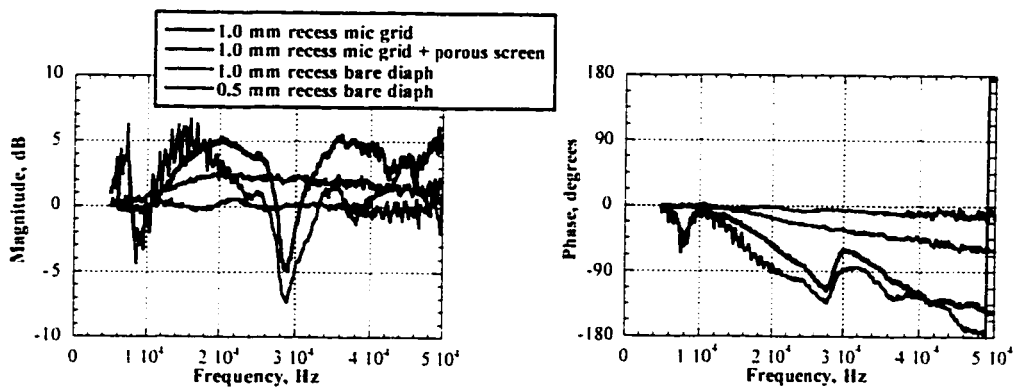


Figure 3.10 Summary of all shallow recess configurations presented for incidence angle of zero degrees

4. PLANE-WAVE REFLECTION AT THE PANEL SURFACE

4.1 Overview

The anechoic chamber experiment was concluded by assessing the response of the test microphone mounted in the flat plate (baseline configuration) relative to the same test microphone, isolated in free field at the same location. First, a single measurement of the baseline configuration (a single test microphone measurement) was acquired on a signal analyzer channel. Figure 4.1 shows the power spectrum of the baseline configuration at zero degrees incidence in the frequency range 5 to 50 kHz. The use of the reference microphone in this setup was eliminated. Then, for the same test microphone position, the array panel was removed and the measurement (a free field microphone) was repeated. Figure 4.2 shows the power spectrum of the free field microphone at zero degrees incidence. To ensure the placement of the test microphone in exactly the same spot for both measurements (baseline and free field), two laser beam pointers, aimed at the center of the test microphone diaphragm, were placed 18 feet in front and 6 feet to either side of the array panel to define the test microphone's location in three dimensional space. Since the placement of the measurement microphone into the field affects free field measurement, the free field correction, which is a theoretical function that accounts for the presence of the microphone in the acoustic field, was applied to the free field measurement.⁹ This correction is based on the physical dimensions of the microphone and the geometry of the microphone in relation to the propagating acoustic waves. Special attention was given to ensure that the noise source stayed constant between the measurements.

The method utilized was the auto-spectra method which requires two separate measurements. The transfer function was calculated from $|H(f)| = \sqrt{\frac{G_{yy}}{G_{xx}}}$ where G_{yy} is the power spectrum of the baseline configuration and G_{xx} is the power spectrum of the same microphone positioned in free field. Note that this method provides no phase information.

4.2 Theory: Plane Wave Reflection

Reference 10 states that sound pressure level is exactly twice or 6 dB higher on the surface than would be obtained if there were no reflections from the surface. In acoustics, the sound pressure level is defined as

$$L_p = 20 * \log \frac{P}{P_{ref}} \quad (4.1)$$

For standard sound pressure reference $P_{ref} = 20 * 10^{-6} \text{ N/m}^2$ (20 μPa). Because of the very wide range of sound power, intensity and pressure encountered in our acoustical environment, it is customary to use the logarithmic scale known as the *decibel scale* to describe these quantities, i. e., to relate the quantity logarithmically to some standard reference. Consider a perfectly reflecting surface as shown on figure 4.3. The sound pressure level incident near the surface and the sound pressure on the surface at $y = 0$ are, respectively

$$L_{p_i} = 20 * \log \frac{P_i}{P_{ref}} \quad (4.2)$$

and

$$L_{p_s} = 20 * \log \frac{P_s}{P_{ref}} \quad (4.3)$$

where i denotes the incident wave and s denotes surface ($y = 0$) conditions. The difference between the incident pressure wave and the incident pressure wave on the surface of the panel can be written as

$$\Delta L_p = L_{p_s} - L_{p_i} \quad (4.4)$$

or substituting

$$\Delta L_p = 20 * \log \frac{P_s}{P_{ref}} - 20 * \log \frac{P_i}{P_{ref}} \quad (4.5)$$

The two expressions on the right hand side of equation (4.5) can be combined to give

$$\Delta L_p = 20 * \log \frac{P_s}{P_i} \quad (4.6)$$

For a perfectly reflecting surface (ref. 10) the incident pressure equals the reflected pressure wave

$$P_i = P_r \quad (4.7)$$

Sound pressure exactly at the surface is

$$P_s = P_i + P_r = 2P_i \quad (4.8)$$

Substituting equation (4.8) into equation (4.6) gives

$$\Delta L_p = 20 * \log \frac{2P_i}{P_i} \quad (4.9)$$

or

$$\Delta L_p = 20 * \log 2 = 6dB \quad (4.10)$$

4.3 Results and Discussion

Figure 4.4 shows a 6 dB sound pressure level increase over the level that would be obtained with a free field standing microphone. Results in this figure were obtained by taking the square root ratio of the power spectrum of baseline configuration (figure 4.1) and the power spectrum of the free field configuration (figure 4.2). Results are observed to an accuracy of ± 1 dB from 5 to 14 kHz and ± 1.5 dB beyond 14 kHz. Results in the current setup can be improved by precise (flush-mount) placement of the test microphone in the array panel. In order to achieve a 0.1 dB accuracy of the final result, for instance, the test microphone needs to be within 0.2 mm of a flush-mount position.

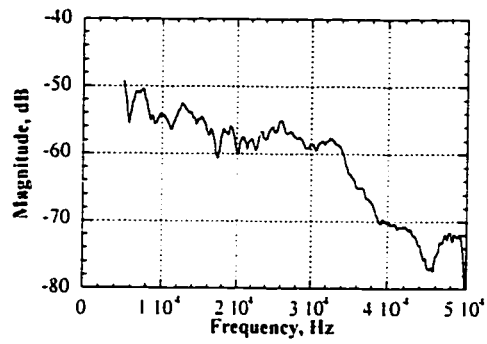


Figure 4.1 Power spectrum of the baseline configuration at zero degrees incidence

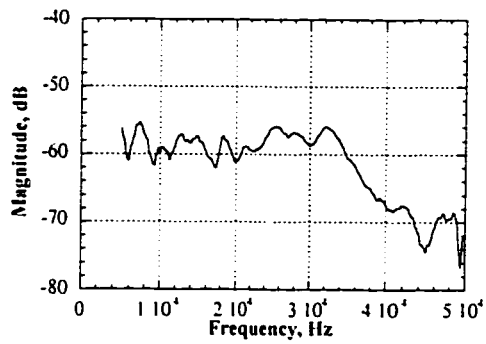


Figure 4.2 Power spectrum of the free field microphone at zero degrees incidence

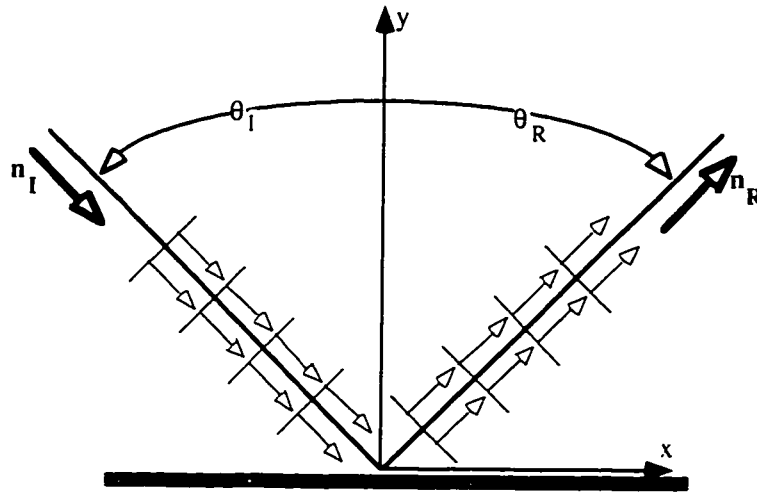


Figure 4.3 Reflection of a plane wave with angle of incidence θ_I and a reflection angle of θ_R at a flat rigid surface

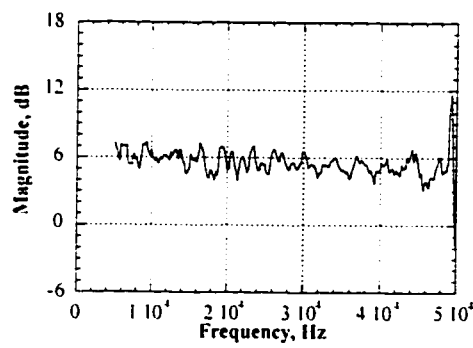


Figure 4.4 Sound pressure level increase of array panel which contains a 19- by 19-inch aluminum piece inclusion

5. SOUND TUBE MEASUREMENTS

This experiment was conducted to measure sound energy absorption coefficient of a one and a half-inch thick sound absorbing foam sample (same foam was used on the NASA Ames 40-element microphone array), a porous screen sample, the combination of one and a half-inch thick foam and the porous screen sample, a one and a half-inch thick fiberglass sample (same fiberglass was used to cover the floor grating of the Ames anechoic chamber), and the empty tube itself. The last case was investigated first to determine the effectiveness of the measuring system. The Standing Wave Apparatus Type 4002, figure 5.1, which is designed for measurements of absorption coefficients of circular cut samples of sound absorbing materials in the frequency range of 800 to 6000 Hz, is utilized to conduct the experiment.

5.1 Sound Tube Test Setup

Figure 5.2 shows a complete arrangement for measurement of acoustic absorption coefficients. The loudspeaker of the Standing Wave Apparatus Type 4002 is fed from the source generator of the dynamic signal analyzer. The fixed sine wave from the analyzer is first amplified with a signal amplifier before being sent to the loudspeaker. The microphone output from the 4002 sound tube apparatus is sent directly to a signal conditioner. Usage of such a signal conditioner allows to set to a desired frequency range. For instance, if a fixed sine wave of 1000 Hz is supplied from the signal analyzer to the loudspeaker, then the frequency range on the band pass filter is set between a high and a low pass filter of 800 Hz and 1250 Hz, respectively. Usage of the band pass filter also gives the experimenter the advantage to avoid unnecessary disturbing effects of

noise outside the desired frequency and to minimize harmonic distortion from the loud speaker. The output from the band pass filter is then connected to an r.m.s. voltmeter for voltage readings and the same signal is split to a digital oscilloscope for display.

5.2 Theoretical Basis for Measurement

Results obtained from the standing wave apparatus are applicable for sound incident normally to the surface of the sample. The frequency range of the method is limited at the lower frequencies by the length of the measuring tube and at the higher frequencies by the diameter of the tube.¹¹

This method uses an incident pressure wave P_i and a sound pressure due to the reflected wave P_r at the same point at the same instant of time disregarding the phase angle between the incident and the reflected waves for determining the sound absorption coefficient.

The two sound waves are, respectively

$$P_i = A \cos 2\pi ft \quad (5.1)$$

$$P_r = B \cos 2\pi f \left(t - \frac{2y}{c} \right). \quad (5.2)$$

The total sound pressure P_y will therefore be

$$P_y = P_i + P_r = A \cos 2\pi ft + B \cos 2\pi f \left(t - \frac{2y}{c} \right). \quad (5.3)$$

The sound pressure will have a maximum value of $(A + B) \cos 2\pi ft$ when $y = \frac{\lambda}{2}$ and a minimum value of $(A - B) \cos 2\pi ft$ when $y = \frac{\lambda}{4}$ where the wavelength $\lambda = \frac{c}{f}$. A

microphone situated at a distance $\frac{\lambda}{2}$ from the sample will therefore receive an alternating sound pressure of frequency f and amplitude $(A + B)$.

The absorption coefficient of the sample can now be defined as the ratio between the energy absorbed by the sample to the total energy incident on the sample and as energy is proportional to the square of the sound pressure then

$$\alpha = 1 - \left(\frac{B}{A}\right)^2. \quad (5.4)$$

5.3 Results and Discussion

Figure 5.3 presents the results for the present investigation. The experimental investigation for the different test material reveal the following conclusion for each test sample.

5.3.1 Empty Tube

This experiment was first initiated by testing the empty tube itself to show the effectiveness of the system. Ideally for the empty tube case, the absorption coefficient will be zero, or it should be very close to zero under normal circumstances. Figure 5.3 (brown solid line) reveal empty test tube results that are very close to having zero absorption coefficient for the frequency range of 800 to 6000 Hz. Having had these results in hand and having shown that the system is very effective even in the high frequencies, four more sample tests were conducted.

5.3.2 Fiberglass Sample

The sound tube result is presented as red solid line in figure 5.3, and figure 5.4(a) shows a pictorial representation of the sample. This material is used to cover the floor grating of the NASA Ames anechoic chamber. This material behaves very similarly to the three-half inch thick foam in the lower frequency ranges, but performs more effectively in higher frequency ranges keeping absorption coefficient between 92 and 98% of total sound energy distribution.

5.3.3 Three-half-inch Thick Foam Sample

The sound tube result is presented as green solid line in figure 5.3, and figure 5.4(b) shows a pictorial representation of the sample. This sample material is used for the NASA Ames 40 element microphone array. As can be seen from figure 5.3, the material behaves very consistently in the high frequency range of 3000 Hz and up, having absorption coefficient of 80% or more with increasing frequency. In the low frequency range, however, the material is shown to have sound energy absorption coefficient of no worse than 50%.

5.3.4 Acoustically Transparent (Porous) Screen

The sound tube result is presented as blue solid line in figure 5.3, and the top portion of figure 5.4(c) is a pictorial representation of the sample. This sample material comprises the outer most component of the 40 element microphone array. Usage of such perforated, coated screen is ideal for minimizing flow-induced noise near the

microphones. This material under investigation, however, is not an effective sound absorbing material. Nevertheless, it contributes to a small amount of sound energy absorption in the frequency range of 800 to 6000 Hz.

5.3.5 Three-half-inch Thick Foam and Porous Screen Combination

The sound tube result is presented as black solid line in figure 5.3, and figure 5.4(c) shows a pictorial representation of the sample. As noted earlier, the one and a half-inch-thick foam fills the air gap between the screen and the microphone surroundings in the 40-element array. This combination sample shows the best results for this experiment, in reducing sound energy contents. The combination starts by absorbing 70% of the sound energy at 800 Hz, reaching a peak value of about 98% at 1750 Hz. The sound energy absorption pattern of Figure 5.3 again dips down to about 70% at 3000 Hz. In the frequency range of 3000 to 6000 Hz, the sound energy absorption is well maintained between 85 and 95% of total sound energy content.

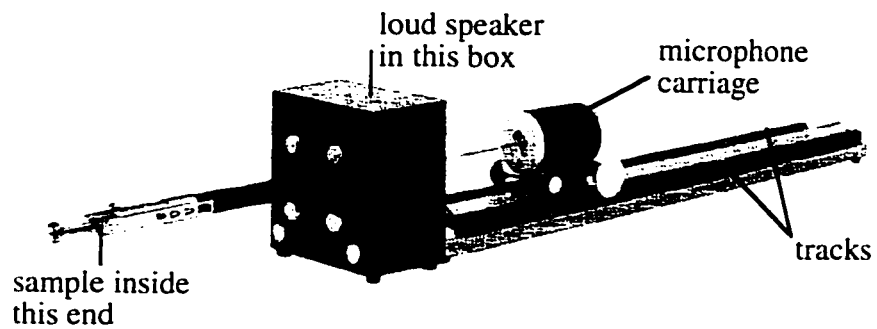


Figure 5.1 Sound tube (standing wave) apparatus shown with the short tube

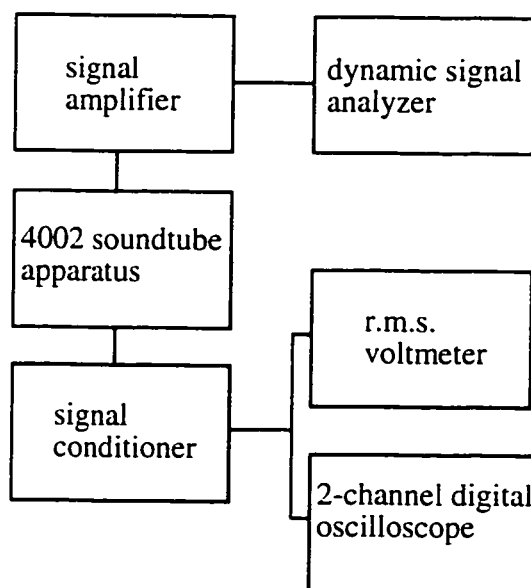


Figure 5.2 Instrumentation flow-chart for the measurement of acoustic absorption coefficient

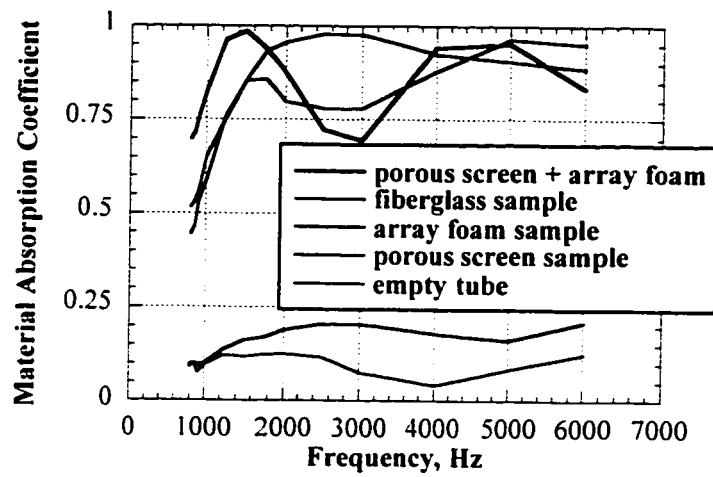


Figure 5.3 Absorption coefficient as a function of frequency for several sound absorbing material

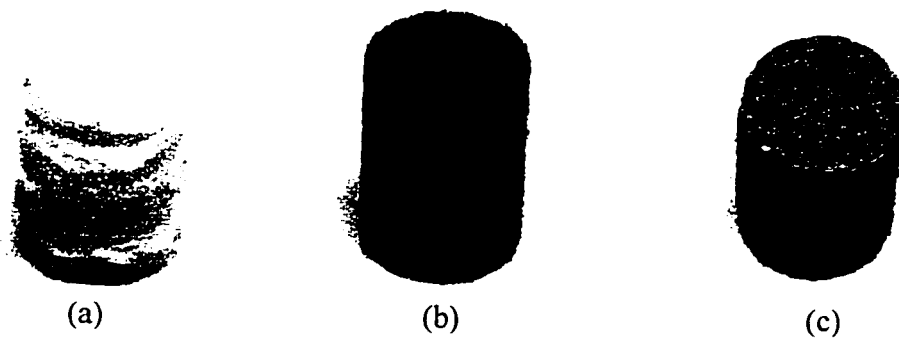


Figure 5.4 (a) Fiberglass sample
 (b) Array foam sample
 (c) Combination of array foam and porous screen sample

6. CONCLUSIONS

An experimental investigation of the acoustic response of a single microphone mounted in a flat plate, which was conducted in the anechoic chamber of the National Full-scale Aerodynamic Complex (NFAC) at NASA Ames Research Center, was outlined and discussed in detail. The purpose of this experiment was to obtain detailed understanding of the acoustic response due to the various microphone installations, including flush-mount and recess-mount configurations. The experiment was performed without flow to determine the acoustic effects of mounting installation schemes on Ames wind tunnel multiple-sensor arrays and to experiment other various microphone installations to identify configurations with least nonuniform regions. All test configurations were related to the baseline configuration, which was a flush mounted microphone with bare diaphragm. Results from this experiment were presented in two parts. First, results for mounting installation schemes on Ames wind tunnel multiple-sensor arrays were presented and analyzed. Second, acoustic studies were also conducted for other various microphone installations to identify configurations with favorable transfer function results.

Degradation of acoustic response from the flush-mounted bare microphone diaphragm baseline configuration were seen in all other installations. Those test configurations which included the use of the sound absorbing foam showed the worst results with unacceptably large amplitude and phase oscillations. Large oscillations and detrimental resonances were also seen in installation configurations which either used the porous screen or the protection grid, or the combination of the two. The results from the 1 mm recess, bare microphone diaphragm showed improved results. The results from the latter and 0.5 mm configurations suggest that flush-mounted, bare microphone

configurations have the most regular magnitude and phase response to an external source as the bare microphone diaphragm is placed near a flush mount. The experiment was concluded by conducting one last configuration to determine the response of the baseline configuration relative to a free field microphone. Sound pressure level was 6 dB higher with the presence of the array panel relative to the same microphone positioned in free field.

Several acoustics tests using phased arrays with both flush-mount and recessed microphone installations have demonstrated that the recess configuration reduces flow-induced noise near the microphones. Moreover, since this noise is largely uncorrelated between the different sensors, the multi-sensor signal processing effectively removes this noise source. Future aeroacoustic tests in Ames wind tunnels will continue to utilize arrays and will use flush mounting of microphones due to the superior acoustic performance.

REFERENCES

1. Jaeger, S. M., Allen, C. S., and Soderman, P. T., "Reduction of Background Noise in the NASA Ames 40- By 80-Foot Wind Tunnel." First Joint CEAS/AIAA Aeroacoustics Conference. June 12-15, 1995.
2. Allen, C. S. and Soderman, P. T., "Aeroacoustic Probe Design for Microphone to Reduce Flow-Induced Self-noise." 15th AIAA Aeroacoustics Conference, AIAA Paper 93-4343. October 1993.
3. Dassen, T. and Holthusen, H. "Design and Testing of a Low Self-Noise Aerodynamic Microphone Forebody." Second Joint AIAA/CEAS Aeroacoustics Conference. May 6-8, 1996.
4. Fields, R. "An Experimental Investigation of Flow-Induced Oscillations of the Brüel & Kjær In-Flow Microphone." Masters Thesis, California Polytechnic University, San Luis Obispo, 1995.
5. Horne, C. and Cooper, D. "Acoustic Array Background Noise Test 7- by 10-ft Wind Tunnel." Posttest Debrief on Preliminary Acoustic Results. NASA Ames Research Center. November 1993.
6. Brüel & Kjær Data Handbook. "Condenser Microphones and Microphone Preamplifiers for Acoustic Measurements." B & K, Denmark. September 1982.
7. Bendat, J. and Piersol, A. "Engineering Applications of Correlation and Spectral Analysis." Second Edition. John Wiley & Sons, Inc. 1993. Pp. 114-115.
8. Horne, C., Hamid, H., and Cooper, D. "Design and Calibration of a Multiple Reflector, In-flow Microphone Array." AIAA 97-0492, AIAA 35th Aerospace Sciences Meeting, Reno, NV, Jan 6-9, 1997.
9. Allen, C., Vandra, K., and Soderman, P. "Microphone Corrections for Accurate In-Flow Acoustic Measurements at High Frequency." CEAS/AIAA 95-150. First Joint CEAS/AIAA Aeroacoustics Conference. Munich, Germany, June 12-15, 1995.
10. Pierce, A. "ACOUSTICS: An Introduction to Its Physical Principles and Applications." McGraw-Hill Book Company. 1981. Pp. 104-106.
11. Brüel & Kjær Instruction Manual. "Standing Wave Apparatus Type 4002." B & K, Denmark. March 1979.